Biophysical Reports

LETTER

Surface tension and viscosity of protein condensates quantified by micropipette aspiration

Huan Wang,[1] Fleurie M. Kelley,[2] Dragomir Milovanovic,[3] Benjamin S. Schuster,[2] and Zheng Shi[1,*]
[1]Department of Chemistry and Chemical Biology and [2]Department of Chemical and Biochemical Engineering, Rutgers University, Piscataway, New Jersey; and [3]Laboratory of Molecular Neuroscience, German Center for Neurodegenerative Diseases, Berlin, Germany

ABSTRACT The material properties of biomolecular condensates have been suggested to play important biological and pathological roles. Despite the rapid increase in the number of biomolecules identified that undergo liquid-liquid phase separation, quantitative studies and direct measurements of the material properties of the resulting condensates have been severely lagging behind. Here, we develop a micropipette-based technique that uniquely, to our knowledge, allows quantifications of both the surface tension and viscosity of biomolecular condensates, independent of labeling and surface-wetting effects. We demonstrate the accuracy and versatility of this technique by measuring condensates of LAF-1 RGG domains and a polymer-based aqueous two-phase system. We further confirm our measurements using established condensate fusion and fluorescence recovery after photobleaching assays. We anticipate the micropipette-based technique will be widely applicable to biomolecular condensates and will resolve several limitations regarding current approaches.

WHY IT MATTERS Biomolecular condensates that arise from liquid-liquid phase separation are often likened to oil droplets in water because of the coexistence of two liquid phases without a membrane boundary. However, oil droplets and biomolecular condensates represent two extremes in the realm of liquid properties. The surface tension of oil droplets is ~1000 times higher, whereas their viscosity is ~1000 times lower, compared with biomolecular condensates. The unique combination of high viscosity and low surface tension makes biomolecular condensates well suited for quantitative micropipette aspiration studies, as demonstrated in this study using condensates of LAF-1 RGG domains. Compared to oil droplets, biomolecular condensates more closely resemble a polymer-based aqueous two-phase system, illustrating how knowledge in polymer physics can guide mechanistic understanding of phase separation in biology.

INTRODUCTION

Biomolecular condensates that arise from liquid-liquid phase separation (LLPS) have recently emerged as a central player in numerous cellular processes (1,2). Surface tension and viscosity are two independent parameters that define the material properties of a liquid (3,4). Gradual increases in the viscosities of biomolecular condensates are often linked to the formation of fibrils that underlie aging-associated diseases (5–10). Quantification of condensate rheology therefore holds promise for unraveling the mechanisms, as well as facilitating therapeutic advances in the treatment of these diseases (11).

The surface tension of biomolecular condensates can also play key physiological roles. Differences in surface tension can lead to layered multiphase condensates, such as the compartmentation in nucleoli (12–14). During autophagy, surface tension determines whether p62 condensates will be sequestered in small droplets or digested as a whole (15). Finally, the nucleation of microtubule branches relies on an instability of TPX2 condensates, driven solely by the condensates' surface tension (16).

Several techniques have been developed to probe either the viscosity or the surface tension of biomolecular condensates (8,12,17–21). The most widely used measure of viscosity relies on fluorescence recovery after photobleaching (FRAP), which is challenging to quantify in the scenario of three-dimensional compartments such as biomolecular condensates (4,22). Measurements of surface tension rely heavily on the fusion kinetics between two condensates (17). Although significant improvements have been made (23,24), the fusion assay is intrinsically limited because only a ratio of surface tension/viscosity can be estimated (12). Therefore,

Submitted June 21, 2021, and accepted for publication July 26, 2021.
*Correspondence: zheng.shi@rutgers.edu
Editor: Erdinc Sezgin.
https://doi.org/10.1016/j.bpr.2021.100011

a user-friendly technique that can directly measure both the surface tension and the viscosity of biomolecular condensates is still missing.

Micropipette aspiration (MPA) has been well established to study the elasticities of liposomes (25,26), polymersomes (27,28), and cells (29,30). However, it has been challenging to apply MPA to quantify liquids. Dimensional analyses on typical MPA experiments show that precise quantifications of both the viscosity and surface tension can only be achieved on liquids with viscosity values (in Pa · s) larger than 2% of their surface tension values (in mN/m) (see Supporting materials and methods for details). Although the criteria is not met by common oil droplets (viscosity: 10^{-3}–10^{-2} Pa · s; surface tension: ~10 mN/m), currently available data suggest that biomolecular condensates and certain aqueous two-phase systems (ATPSs) (viscosity: 10^{-1}–10^{3} Pa · s; surface tension: 10^{-4}–10^{-1} mN/m) are well poised for quantitative MPA studies (Fig. 1).

Here, we demonstrate the application of MPA to quantify the viscosity and surface tension of liquid condensates. We calibrated our method using a PEG-dextran ATPS (35). This allowed us to develop a linear model to extract the material properties of condensates from their responses to MPA. We applied this technique to quantify condensates formed by the RGG domain, a well-known RNA binding region of the P granule RNA helicase LAF-1 that undergoes LLPS (18,36). We further confirmed our viscosity and surface tension measurements by FRAP and fusion assays, respectively. Our results suggest that the material properties of protein condensates are closer to the ATPS than to oil droplets in water. MPA represents an active microrheology technique that can simultaneously quantify independent properties of biomolecular condensates, insensitive to common sources of artifacts such as labeling, photobleaching, and wetting effects of proteins.

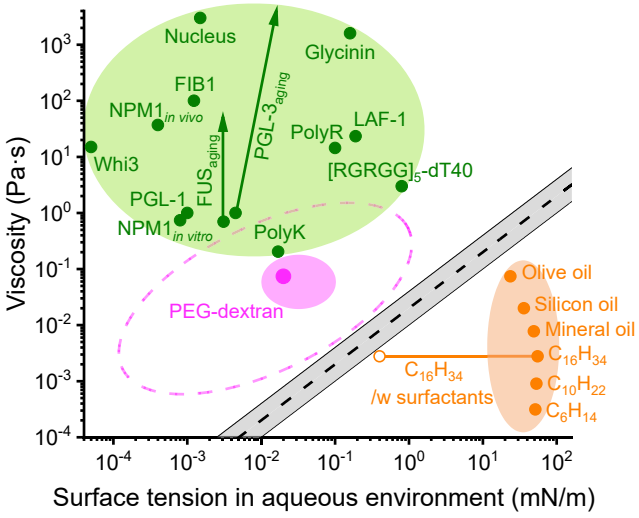

FIGURE 1 Viscosity and surface tension of liquids. Viscosity and surface tension of biomolecular condensates in aqueous buffer (*green*, *arrows* represent changes of properties over time) and common "oil droplets" in water are shown (*orange*, *open circle* and *line* represent the minimum and change of hexadecane surface tension in the presence of surfactants (31)). The gray belt represents an estimated boundary above which MPA will be well suited for viscosity and surface tension measurements ($\eta = 0.02\times\gamma$ is plotted as the *black dashed line*; the *gray region* represents $\eta = 0.01\times\gamma$ to $\eta = 0.04\times\gamma$; see Supporting materials and methods for details). Viscosity and surface tension of the dextran-rich condensates (in PEG-dextran ATPS) measured in this study are shown as the magenta circle. Literature values for dextran-rich condensates are represented by the dashed circle (32–34), with compositions comparable with the one used in this study highlighted in light magenta. See Table S1 for values and references used in this plot.

Results

Calibration of MPA with PEG-dextran ATPS

To study the relation between the stress and strain rate of a liquid, a critical aspiration pressure P_γ, determined by the surface tension (γ) of the condensate, needs to be reached. At aspiration pressures (P_{asp}) greater than P_γ, the condensate will flow into the micropipette (Fig. 2 *a*; we define suction pressures as positive). For a Newtonian fluid, the pressure difference and the shear rate are linearly related via the condensate's viscosity (η) (37):

$$P_{asp} = M \times \eta \times S + P_\gamma. \quad (1)$$

Here, M is a unitless dissipation factor that corresponds to the radial collapse of the condensate during aspiration (37), $S = d(L_p/R_p)/dt$ is the shear rate, L_p is the aspiration length, and R_p is the radius of the micropipette. The critical pressure is $P_\gamma = 2\gamma(H - 1/R_c)$, with H representing the mean curvature of the liquid interface in the micropipette (we define the curvature illustrated in Fig. 2 *a* as positive). The unaspirated portion of the condensate is approximated by a sphere of radius R_c. Equation 1 is valid when $\Delta L_p R_p^2/R_c^3 << 1$, with M independent of geometrical factors in the MPA system (37). When $\Delta L_p R_p^2/R_c^3 \sim 1$, geometrical dependence of M and dissipation in the micropipette will need to be considered. In our experiments, $\Delta L_p R_p^2/R_c^3 < 0.05$.

R_c, L_p, R_p, and H describe the shape of the aspirated condensate and are readily available through microscopy. However, the unitless dissipation constant M must be determined experimentally by aspirating liquids of known viscosities (37). Then, by measuring S under different P_{asp}, the viscosity and surface tension of an unknown liquid condensate can be quantified from the slope and intercept, respectively, of Eq. 1.

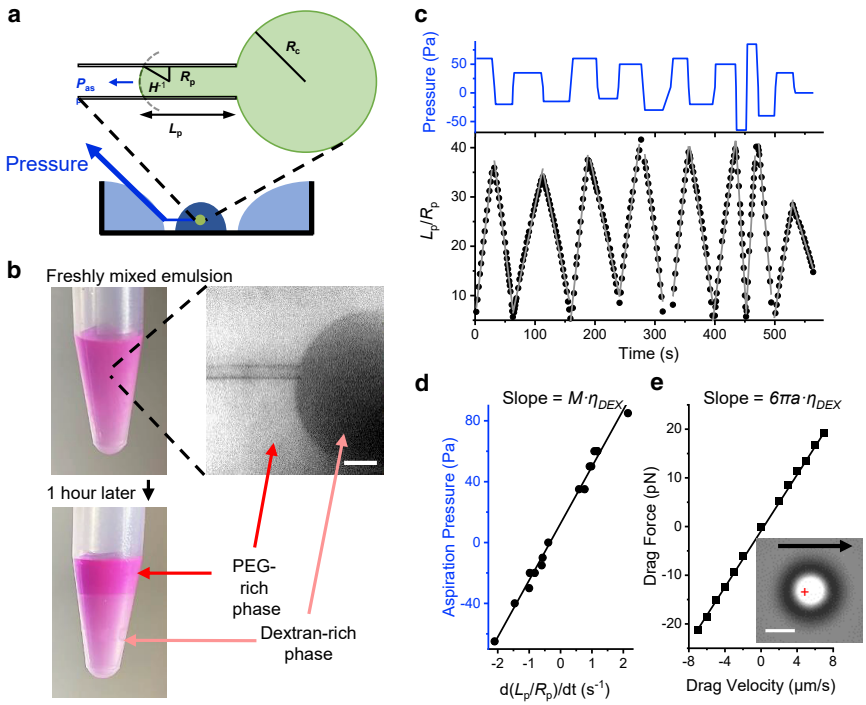

FIGURE 2 Micropipette aspiration of dextran-rich condensates. (*a*) Illustration of the micropipette aspiration system: dark blue, sample; light blue, water used for minimizing evaporation; green, a pipette-aspirated condensate; P_{asp}, aspiration pressure; R_p, pipette radius; L_p, aspiration length; R_c, radius of condensate outside the pipette. H: mean curvature of the liquid interface in the micropipette. (*b*) An emulsion of PEG-dextran (*upper*) undergoes bulk LLPS after creaming for 1 h (*lower*). Scale bars, 20 μm. (*c*) Aspiration pressure (*upper*) and normalized aspiration length (*lower*) during MPA. Gray lines: linear fits of the normalized aspiration length for each pressure step. (*d*) P_{asp} of each step plotted against the corresponding shear rate (slopes of the *gray lines* in *c*). (*e*) Viscosity determination by optical dragging. Inset image: a trapped polystyrene particle dragged at 5 μm/s (*arrow*) in the dextran-rich phase. Cross: trap-center. Scale bars, 2 μm. Linear fits: $R^2 = 0.990$ for (*d*) and 0.999 for (*e*).

To calibrate M with liquids that are appropriate for MPA (Fig. 1), we chose an ATPS composed of PEG (8000 Da) and dextran (500,000 Da) (15,32,38). Under a range of concentrations, mixtures of PEG and dextran will phase separate into emulsions of micrometer-sized droplets (Fig. S1 *a*). Rhodamine-B was included to identify the condensates microscopically. This mixture produced a labeled emulsion that is stable on the timescale of MPA experiments (~10 min) but undergoes bulk phase separation after 1–2 h (Fig. 2 *b*).

With careful control of water evaporation (Fig. S2), next we applied MPA to samples of limited volumes (20–30 μL). Stepwise aspiration pressures were applied to dextran-rich condensates, and the aspiration length was found to change linearly under each pressure step (Figs. 2 *c* and S1 *b*). The resulting relation between the aspiration pressure and the condensate flow (Fig. 2 *d*) agrees well with predictions from Eq. 1. The slope $dP_{asp}/dS = 37.0 \pm 0.7$ Pa · s (n = 6; mean ± standard error of the mean for all values reported herein) represents the viscosity of the dextran-rich phase multiplied by M (Eq. 1). We then directly measured the viscosity by dragging an optically trapped particle within the dextran-rich phase (Fig. 2 *e*). The measured viscosity of the dextran-rich phase (74 ± 4 mPa · s) agreed with bulk viscometer measurements (Supporting materials and methods), giving $M = 500 \pm 30$, a value that can be directly applied when quantifying the viscosity of other liquid condensates via independent MPA setups, provided $\Delta L_p R_p^2/R_c^3 << 1$. Additionally, the intercept from the P_{asp}-S relation corresponds to a surface tension of 0.02 ± 0.01 mN/m (Eq. 1), in agreement with the literature (32,34).

Surface tension and viscosity of LAF-1 RGG condensates quantified by MPA

LAF-1 is one of the first well-studied proteins that undergoes LLPS, mediated mainly by its intrinsically disordered N-terminal RGG domain (4,18,19,22,36). The RGG domain consists of the first 168 residues of LAF-1 and is especially rich in glycine and arginine (39). We applied MPA to a tandem RGG domain that robustly undergoes LLPS (Supporting materials and methods; hereafter named RGG condensates) (36). Unlike dextran-rich condensates, RGG condensates fully wet the inner wall of the micropipette, requiring a negative (ejection) pressure P_γ to balance the capillary effect (Fig. 3 *a*; Video S1; $H \approx -1/R_p$). Beyond P_γ, the aspiration length changed linearly under each pressure step (Fig. 3 *b*), indicating a lack of condensate elasticity at the timescale we were probing (>1 s). After the initial entry steps, the shear rate S increased linearly with P_{asp} (Figs. 3 *c*, S3, and S4). The slope corresponded to a viscosity of 1.62 ± 0.18 Pa · s (n = 11). As expected from the wetting behavior, the intercept of P_{asp} vs. S was negative, and the corresponding surface tension was 0.159 ± 0.010 mN/m (n = 11). The viscosity and surface tension measured through MPA are in agreement with previous estimates for condensates of LAF-1 RGG using FRAP and condensate fusion assays (39).

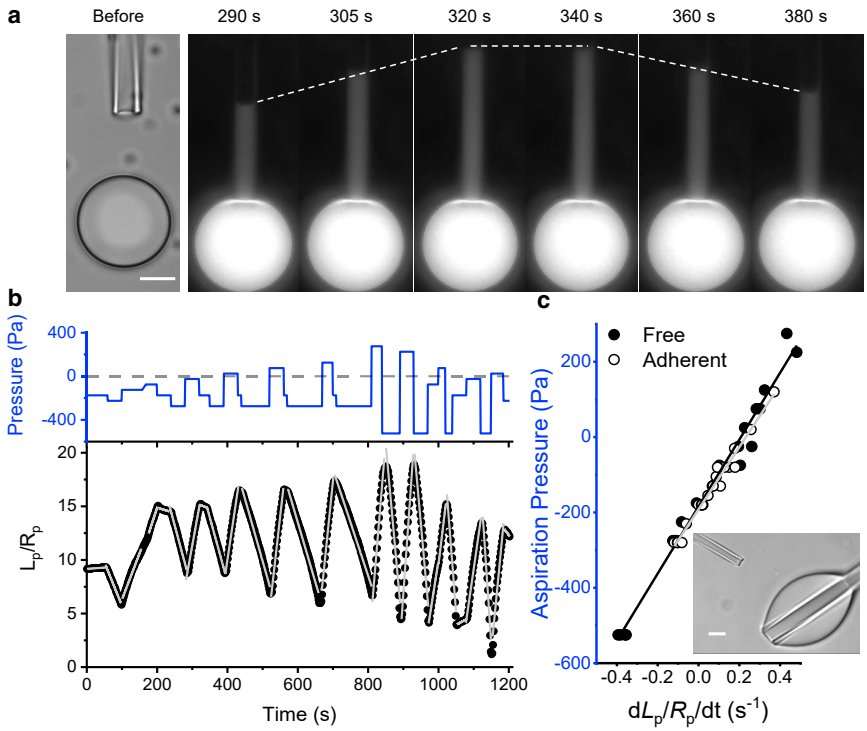

FIGURE 3 MPA of RGG condensates. (*a*) Left: transmitted light image of an RGG condensate with a nearby micropipette. Right: time-lapse fluorescent images of the RGG condensate under three aspiration pressures: −25 Pa (290–320 s), −175 Pa (320–340 s), and −275 Pa (340–380 s). Dashed lines trace the change of L_p. (*b*) Aspiration pressure (*upper*) and normalized aspiration length (*lower*) during MPA. Dashed line: zero pressure. Gray lines: linear fits of the normalized aspiration length for each pressure step. (*c*) P_{asp} of each step plotted against the corresponding shear rates for a free condensate (*closed*, see *a*) and a condensate strongly adhered to a glass pipette (*open*, *inset image*). Linear fits to the data are shown as black (slope: 890 ± 30 Pa · s, intercept: −184 ± 7 Pa, R^2 = 0.982) and gray (slope: 830 ± 30 Pa · s, intercept: −192 ± 4 Pa, R^2 = 0.976) lines, respectively. All scale bars, 10 μm.

Compared with currently available methods for condensate rheology and surface tension measurements, MPA has significant advantages. First, many proteins tend to wet and adsorb onto solid surfaces (4,16,23,24,40). Although potentially mediating important biological processes (15,16,40,41), this wetting effect can introduce significant artifacts in measurements that rely on the fusion kinetics or morphology of condensates (12,23,24). In our experiments, adhesion between RGG condensates and the glass bottom dish can be prevented by coating the glass with Pluronic F-127 (36). However, the same coating procedure does not necessarily work for other protein condensates or glass surfaces. To study the effect of wetting in MPA measurements, we carried out experiments to compare sedimented condensates that were weakly attached to the bottom coverglass of a coated dish (Fig. 3 *a*) with condensates that were strongly adhered to a bare glass pipette (Fig. 3 *c*, *inset*; n = 5). Adhesion to glass led to nonspherical condensates outside the aspiration pipette (Videos S2 and S3); however, P_{asp} vs. S relations measured under these two different configurations were not significantly different (Fig. 3 *c*; p = 0.83 for viscosity and p = 0.45 for surface tension, Student's *t*-test). The insensitivity of MPA to the wetting between condensate and glass is expected from Eq. 1, for which the contribution of R_c is negligible when $|R_c^{-1}| << H$, as in our experiments. Additionally, fluorescent labeling of the protein is not necessary for MPA as long as the condensate-buffer interfaces can be resolved (Figs. S1 *c* and S4; Video S3). For the same reasons, MPA measurements are insensitive to photobleaching and can be easily combined with fluorescence-based studies (24,42). Finally, MPA does not require highly specialized instrumentation or the incorporation particles to the condensate (8,18), further expanding the applicability of this technique.

Estimation of RGG condensate properties through FRAP and fusion assays

To confirm the accuracy of the surface tension and viscosity of RGG condensates measured by MPA, we first adopted an improved version of the condensate fusion assay (23,24). Two optically trapped RGG condensates were manipulated to encounter each other, and the subsequent fusion process was recorded (Fig. 4, *a and b*; n = 76 pairs). A linear relation was observed between the fusion time and the size of the condensates (Fig. 4 *c*). The slope, which scales with the inverse capillary velocity η/γ, was 0.016 ± 0.002 s/μm, in agreement with the MPA measurements (η/γ = 0.010 ± 0.001 s/μm).

We then used FRAP to estimate the viscosity of RGG condensates. A circular region within RGG condensates was photobleached, and the three-dimensional diffusion coefficient (D = 0.018 μm^2/s) was calculated based on the half-recovery time (Fig. 4 *d*, n = 42; Eqs. S7a and S8b) (22). Combined with an estimate of the protein hydrodynamic radius, we obtained a viscosity

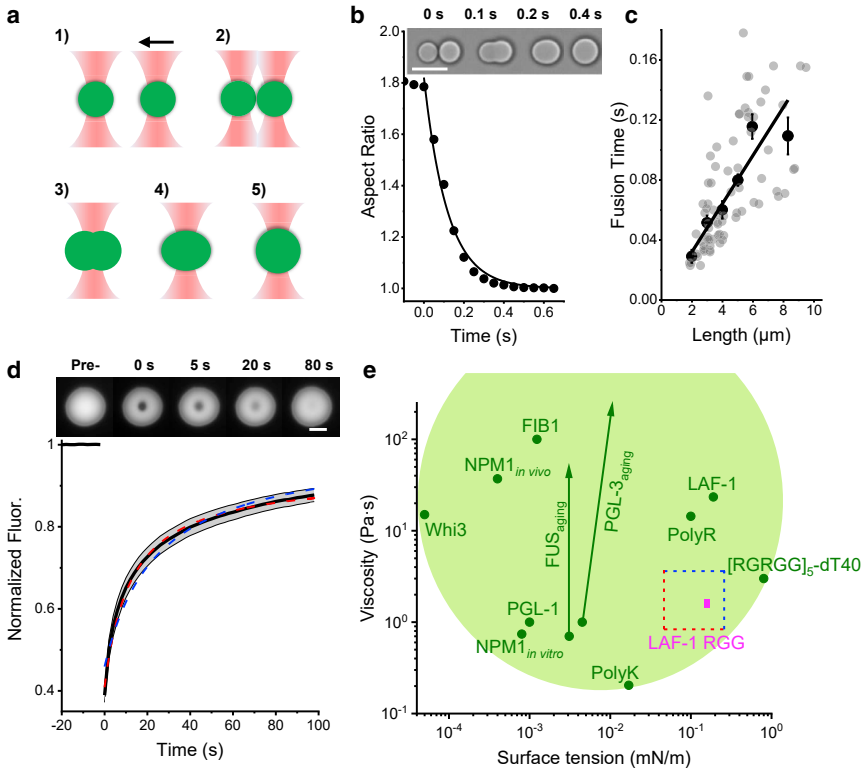

FIGURE 4 Surface tension and viscosity of RGG condensates estimated from condensate fusion and FRAP. (*a*) (*1–5*): Illustration of the condensate fusion experiment using dual-optical traps. (*b*) Fusion of two RGG condensates (*inset images*) quantified as a decrease of the overall aspect ratio to 1. The curve is an exponential fit. (*c*) The fusion time of RGG condensates versus the condensates' length. Gray and black circles are individual and binned fusion experiments, respectively. Line: weighted linear fit to the binned data ($R^2 = 0.902$). (*d*) FRAP measurements within RGG condensates. Inset images show a representative experiment. Red dash represents the fit to a model in which an immobile fraction of the protein was allowed (Eq. S7a; $R^2 = 0.995$). Blue dash represents the fit to a model in which all proteins were assumed to be mobile (Eq. S7b; $R^2 = 0.966$). (*e*) Zoom-in of Fig. 1, with MPA-measured RGG condensate viscosity (1.62 ± 0.18 Pa · s) and surface tension (0.159 ± 0.010 mN/m) represented by the magenta box. The range of viscosity and surface tension estimated from FRAP and condensate fusion are represented by the dashed box. The horizontal red dashed line ($\eta = 0.8$ Pa · s) represents viscosity calculated assuming the presence of immobile proteins in a two-dimensional model (Eqs. S7a and S8a). The vertical red dashed line represents surface tension calculated using $\eta = 0.8$ Pa · s and the upper bound of inverse capillary velocity ($\eta/\gamma = 0.018$ s/μm). The horizontal blue dashed line ($\eta = 3.6$ Pa · s) represents viscosity calculated assuming the absence of immobile fraction in a three-dimensional model (Eqs. S7b and S8b). The vertical blue dashed line represents surface tension calculated using $\eta = 3.6$ Pa · s and the lower bound of inverse capillary velocity ($\eta/\gamma = 0.014$ s/μm). All error bars are mean $\pm$ standard error of the mean; all scale bars represent 10 μm.

of 1.8 Pa · s, comparable with the MPA result. We noticed that viscosity values between 0.8 and 3.6 Pa · s can be extracted from FRAP, depending on the extract model of choice (Fig. 4 *e*). The agreement between FRAP- and MPA-based viscosity measurements on the same RGG condensates independently confirmed that our calibrated *M* value (500 $\pm$ 30) is accurate within a factor of 2.

Discussion

In this study, we only explored condensates that behave as Newtonian fluids at the timescale of our MPA measurements (>1 s). We demonstrated that MPA can be applied to simultaneously quantify the surface tension and viscosity of RGG condensates. However, several other biomolecule condensates are known to be viscoelastic or gel-like (8,10,20). When applying stepwise changes in aspiration pressure to viscoelastic condensates, immediate elastic responses followed by nonlinear creep compliances in the aspiration length would be expected (43). Although these were not observed on either dextran-rich (Fig. 2 *c*) or RGG condensates (Fig. 3 *b*), it is highly probable that condensates made of complex multidomain proteins can exhibit prominent viscoelastic features. Generalized viscoelastic models will need to be evoked to fit the time-dependent aspiration lengths when applying our MPA protocol to viscoelastic condensates. Specifically, this involves replacing the linear fitting to the aspiration length (such as in the *lower panels* of Figs. 2 *c* and 3 *b*) with exponential or power-law fittings (44). It is also possible to apply a sinusoidally oscillating pressure to an aspirated condensate, for which the phase delay in the response of aspiration length will inform the condensate's frequency-dependent viscoelasticity (20,45). Because of the inertia of the aspiration system, it is challenging to operate MPA faster than 10 Hz. However, it is currently unclear whether the high-frequency elastic response of biomolecular condensates would have direct biological relevance.

RGG condensates fuse quickly (inverse capillary velocity ~0.01 s/μm) with >90% of the constituting proteins moving freely, consistent with their liquid behavior during MPA. However, many biomolecular condensates can take more than 100 s to fuse (15,46) while exhibiting small fractions (<50%) of mobile proteins (3,10,47). In the latter cases, MPA measurements will be essential to clarify confusion

around the condensates' material properties. For example, in a “gel-like” multicomponent condensate (10), viscoelastic properties of the condensate can be measured by MPA without necessarily knowing its molecular constituents, in contrast with assays based on fluorescent labeling.

The unambiguous quantification of RGG condensates through MPA further iterates the contrasting material properties of biomolecular condensates and oil droplets (Fig. 1). For example, mineral oil has a surface tension 300-fold higher than that of RGG condensates, whereas its viscosity is more than 200-fold lower. The cause of this drastic difference between biomolecular condensates and oil droplets has not been studied in detail. However, it is conceivable that the large size of biopolymers compared with those of typical oil molecules plays a role in determining both viscosity and surface tension (17). The difference can also arise from intermolecular interactions. For example, the strong hydrophobicity of oil-like molecules contributes to their high (10 mN/m) surface tensions, whereas biopolymers often tend to form hydrogen bonds with water (48).

The contrast between biomolecular condensates and oil droplets can affect scientists' intuition about phase separation in biology; the known capillary velocities for biomolecular condensates have a median value of 1 μm/s, with several examples below 0.01 μm/s (Fig. 4 *e*). These capillary velocities correspond to a complete fusion between micron-sized condensates in seconds to minutes. These fusion rates can leave a strong impression of liquid-like condensates when observed under a microscope. However, the liquid behavior becomes nonintuitive when these micron-sized condensates are scaled to the macroscopic world. For example, under a capillary velocity of 0.01–1 μm/s, it will take hours to weeks for droplets of centimeter size to fuse together, a rate at which the liquidity of the droplets may become debatable (49).

In our protein condensates, the helicase domain and disordered C-terminal prion-like domain of the full length LAF-1 were replaced by a second copy of the N-terminal RGG domain (36). Comparing our measurements of RGG condensates and literature reports on LAF-1 condensates (18), the viscosity of RGG condensates is more than 10-fold smaller than that of LAF-1 condensates, whereas their surface tensions are comparable (Fig. 4 *e*). These results point to a potential role of the helicase and C-terminal domains in uniquely controlling the viscosity of LAF-1 condensates. More generally, surface tension and viscosity are tunable through intermolecular interactions. Thus, a future direction will be to systematically dissect how protein sequence and biochemical environment affect the material properties of biomolecular condensates (50).

Importantly, by carefully implementing a whole-cell patch-clamp configuration (51), the demonstrated MPA protocol could be applied to study large (>2 μm in diameter) cytosolic biomolecular condensates *in vivo*. MPA setups are readily available in electrophysiology and biomechanics labs, making it easily adaptable for studying the material properties of biomolecular condensates in the broader biological and chemical communities.

SUPPORTING MATERIAL

Supporting material can be found online at https://doi.org/10.1016/j.bpr.2021.100011.

AUTHOR CONTRIBUTIONS

Z.S., B.S.S., and D.M. conceived the project. H.W. and Z.S. carried out the experiments and analyzed the data. F.M.K. purified the proteins. Z.S., H.W., B.S.S., and D.M. wrote the manuscript.

ACKNOWLEDGMENTS

We thank Howard Stone and Lin Guo for critical evaluation of the manuscript. We thank Ehsan Ateﬁ, Ningwei Li, Rumiana Dimova, Christine Keating, Dennis Discher, Marina Feric, Roland Knorr, Frank Jülicher, and Rick Remsing for helpful discussions. We thank Gayatri Ganeshan, Steven Arnold, and Roberto Sul for careful proofreading. We also thank Andy Nieuwkoop and his lab for helping with materials and storage space.

Z.S. and B.S.S. are supported by Rutgers University startup funds. F.M.K. is supported by National Institutes of Health Award T32 GM135141. D.M. is supported by the German Research Foundation (MI 2104 and SFB 1286) and the German Academic Exchange Service (PPE 2021).

DECLARATION OF INTERESTS

The authors declare no competing interests.

REFERENCES

1. Shin, Y., and C. P. Brangwynne. 2017. Liquid phase condensation in cell physiology and disease. *Science.* 357:eaaf4382.
2. Banani, S. F., H. O. Lee, …, M. K. Rosen. 2017. Biomolecular condensates: organizers of cellular biochemistry. *Nat. Rev. Mol. Cell Biol.* 18:285–298.
3. Bracha, D., M. T. Walls, and C. P. Brangwynne. 2019. Probing and engineering liquid-phase organelles. *Nat. Biotechnol.* 37:1435–1445.
4. Schuster, B. S., R. M. Regy, …, J. Mittal. 2021. Biomolecular condensates: sequence determinants of phase separation, microstructural organization, enzymatic activity, and material properties. *J. Phys. Chem. B.* 125:3441–3451.
5. Mathieu, C., R. V. Pappu, and J. P. Taylor. 2020. Beyond aggregation: pathological phase transitions in neurodegenerative disease. *Science.* 370:56–60.

6. Nedelsky, N. B., and J. P. Taylor. 2019. Bridging biophysics and neurology: aberrant phase transitions in neurodegenerative disease. *Nat. Rev. Neurol.* 15:272–286.
7. Alberti, S., and D. Dormann. 2019. Liquid–liquid phase separation in disease. *Annu. Rev. Genet.* 53:171–194.
8. Jawerth, L., E. Fischer-Friedrich, …, F. Jülicher. 2020. Protein condensates as aging Maxwell fluids. *Science.* 370:1317–1323.
9. Guo, L., H. J. Kim, …, J. Shorter. 2018. Nuclear-import receptors reverse aberrant phase transitions of RNA-binding proteins with prion-like domains. *Cell.* 173:677–692.e20.
10. Putnam, A., M. Cassani, …, G. Seydoux. 2019. A gel phase promotes condensation of liquid P granules in *Caenorhabditis elegans* embryos. *Nat. Struct. Mol. Biol.* 26:220–226.
11. Guo, L., C. M. Fare, and J. Shorter. 2019. Therapeutic dissolution of aberrant phases by nuclear-import receptors. *Trends Cell Biol.* 29:308–322.
12. Feric, M., N. Vaidya, …, C. P. Brangwynne. 2016. Coexisting liquid phases underlie nucleolar subcompartments. *Cell.* 165:1686–1697.
13. Fisher, R. S., and S. Elbaum-Garfinkle. 2020. Tunable multiphase dynamics of arginine and lysine liquid condensates. *Nat. Commun.* 11:4628.
14. Yu, H., S. Lu, …, D. W. Cleveland. 2021. HSP70 chaperones RNA-free TDP-43 into anisotropic intranuclear liquid spherical shells. *Science.* 371:eabb4309.
15. Agudo-Canalejo, J., S. W. Schultz, …, R. L. Knorr. 2021. Wetting regulates autophagy of phase-separated compartments and the cytosol. *Nature.* 591:142–146.
16. Setru, S. U., B. Gouveia, …, S. Petry. 2021. A hydrodynamic instability drives protein droplet formation on microtubules to nucleate branches. *Nat. Phys.* 17:493–498.
17. Brangwynne, C. P., C. R. Eckmann, …, A. A. Hyman. 2009. Germline P granules are liquid droplets that localize by controlled dissolution/condensation. *Science.* 324:1729–1732.
18. Elbaum-Garfinkle, S., Y. Kim, …, C. P. Brangwynne. 2015. The disordered P granule protein LAF-1 drives phase separation into droplets with tunable viscosity and dynamics. *Proc. Natl. Acad. Sci. USA.* 112:7189–7194.
19. Taylor, N., S. Elbaum-Garfinkle, …, C. P. Brangwynne. 2016. Biophysical characterization of organelle-based RNA/protein liquid phases using microfluidics. *Soft Matter.* 12:9142–9150.
20. Jawerth, L. M., M. Ijavi, …, E. Fischer-Friedrich. 2018. Salt-dependent rheology and surface tension of protein condensates using optical traps. *Phys. Rev. Lett.* 121:258101.
21. Caragine, C. M., S. C. Haley, and A. Zidovska. 2018. Surface fluctuations and coalescence of nucleolar droplets in the human cell nucleus. *Phys. Rev. Lett.* 121:148101.
22. Taylor, N. O., M. T. Wei, …, C. P. Brangwynne. 2019. Quantifying dynamics in phase-separated condensates using fluorescence recovery after photobleaching. *Biophys. J.* 117:1285–1300.
23. Alshareedah, I., G. M. Thurston, and P. R. Banerjee. 2021. Quantifying viscosity and surface tension of multicomponent protein-nucleic acid condensates. *Biophys. J.* 120:1161–1169.
24. Ghosh, A., and H. X. Zhou. 2020. Determinants for fusion speed of biomolecular droplets. *Angew. Chem. Int. Ed. Engl.* 59:20837–20840.
25. Shi, Z., and T. Baumgart. 2015. Membrane tension and peripheral protein density mediate membrane shape transitions. *Nat. Commun.* 6:5974.
26. Evans, E., and W. Rawicz. 1990. Entropy-driven tension and bending elasticity in condensed-fluid membranes. *Phys. Rev. Lett.* 64:2094–2097.
27. Luo, Q., Z. Shi, …, S. J. Park. 2016. DNA island formation on binary block copolymer vesicles. *J. Am. Chem. Soc.* 138:10157–10162.
28. Discher, B. M., Y. Y. Won, …, D. A. Hammer. 1999. Polymersomes: tough vesicles made from diblock copolymers. *Science.* 284:1143–1146.
29. Hochmuth, R. M. 2000. Micropipette aspiration of living cells. *J. Biomech.* 33:15–22.
30. Lee, L. M., and A. P. Liu. 2014. The application of micropipette aspiration in molecular mechanics of single cells. *J. Nanotechnol. Eng. Med.* 5:0408011–0408016.
31. Chen, H., L. Han, …, Z. Ye. 2004. The interfacial tension between oil and gemini surfactant solution. *Surf. Sci.* 552:L53–L57.
32. Atefi, E., J. A. Mann, Jr., and H. Tavana. 2014. Ultralow interfacial tensions of aqueous two-phase systems measured using drop shape. *Langmuir.* 30:9691–9699.
33. Carrasco, F., E. Chornet, …, J. Costa. 1989. A generalized correlation for the viscosity of dextrans in aqueous solutions as a function of temperature, concentration, and molecular weight at low shear rates. *J. Appl. Polym. Sci.* 37:2087–2098.
34. Liu, Y., R. Lipowsky, and R. Dimova. 2012. Concentration dependence of the interfacial tension for aqueous two-phase polymer solutions of dextran and polyethylene glycol. *Langmuir.* 28:3831–3839.
35. Crowe, C. D., and C. D. Keating. 2018. Liquid-liquid phase separation in artificial cells. *Interface Focus.* 8:20180032.
36. Schuster, B. S., E. H. Reed, …, D. A. Hammer. 2018. Controllable protein phase separation and modular recruitment to form responsive membraneless organelles. *Nat. Commun.* 9:2985.
37. Drury, J. L., and M. Dembo. 1999. Hydrodynamics of micropipette aspiration. *Biophys. J.* 76:110–128.
38. Helfrich, M. R., L. K. Mangeney-Slavin, …, C. D. Keating. 2002. Aqueous phase separation in giant vesicles. *J. Am. Chem. Soc.* 124:13374–13375.
39. Schuster, B. S., G. L. Dignon, …, J. Mittal. 2020. Identifying sequence perturbations to an intrinsically disordered protein that determine its phase-separation behavior. *Proc. Natl. Acad. Sci. USA.* 117:11421–11431.
40. Su, X., J. A. Ditlev, …, R. D. Vale. 2016. Phase separation of signaling molecules promotes T cell receptor signal transduction. *Science.* 352:595–599.
41. Milovanovic, D., Y. Wu, …, P. De Camilli. 2018. A liquid phase of synapsin and lipid vesicles. *Science.* 361:604–607.
42. Alberti, S., A. Gladfelter, and T. Mittag. 2019. Considerations and challenges in studying liquid-liquid phase separation and biomolecular condensates. *Cell.* 176:419–434.
43. Mitchell, J. R. 1980. The rheology of gels. *J. Texture Stud.* 11:315–337.
44. Moazzeni, S., Y. Demiryurek, …, H. Lin. 2021. Single-cell mechanical analysis and tension quantification via electrodeformation relaxation. *Phys. Rev. E.* 103:032409.
45. Sakai, A., Y. Murayama, and M. Yanagisawa. 2020. Cyclic micropipette aspiration reveals viscoelastic change of a gelatin microgel prepared inside a lipid droplet. *Langmuir.* 36:5186–5191.
46. Zhang, H., S. Elbaum-Garfinkle, …, A. S. Gladfelter. 2015. RNA controls PolyQ protein phase transitions. *Mol. Cell.* 60:220–230.
47. Hoffmann, C., R. Sansevrino, …, D. Milovanovic. 2021. Synapsin condensates recruit alpha-synuclein. *J. Mol. Biol.* 433:166961.
48. Israelachvili, J. N. 2015. Intermolecular and Surface Forces. Academic Press, Cambridge, MA.
49. Edgeworth, R., B. J. Dalton, and T. Parnell. 1984. The pitch drop experiment. *Eur. J. Phys.* 5:198–200.
50. Peeples, W., and M. K. Rosen. 2021. Mechanistic dissection of increased enzymatic rate in a phase-separated compartment. *Nat. Chem. Biol.* 17:693–702.
51. Zhang, H., E. Reichert, and A. E. Cohen. 2016. Optical electrophysiology for probing function and pharmacology of voltage-gated ion channels. *eLife.* 5:e15202.